www.springer.com/41230
https://doi.org/10.1007/s41230-022-9022-z

Plasticity improvement of $(Cu_{43}Zr_{48}Al_9)_{98}Y_2$ bulk metallic glass composites by dispersed Ta particles

***Ke Yang, Bing Li, Xin Wang, and Xin-hui Fan**
School of Materials Science and Chemical Engineering, Xi'an Technological University, Xi'an 710021, China

Abstract: $(Cu_{43}Zr_{48}Al_9)_{98}Y_2$-based bulk metallic glass composites (BMGCs) with dispersed Ta particles (3vol.%, 6vol.%, 9vol.%) were successfully fabricated through suction casting. The thermal properties, microstructure, and mechanical properties of the BMGCs were systematically investigated. Ta particles are homogeneously dispersed in the amorphous matrix. Ta particle reinforced BMGCs exhibit similar thermal properties and glass-forming ability with the $(Cu_{43}Zr_{48}Al_9)_{98}Y_2$ base BMG. Compression test results show that the BMGC with 9vol.% Ta particles has superior mechanical performance with up to 15.7% compressive plastic strain, 2,216 MPa yield strength, and 2,260 MPa fracture strength at room temperature. These homogeneously distributed Ta particles act as discrete obstacles in the amorphous matrix, restricting the highly localized shear band. This results in the formation of multiple shear bands around the Ta-rich particles, which lowers the stress concentration, allowing the shear band to propagate further and improve plasticity.

Keywords: bulk metallic glass; composites; Ta particles; mechanical properties; microstructure

CLC numbers: TG139$^+$.8 **Document code:** A **Article ID:** 1672-6421(2022)03-275-06

1 Introduction

CuZr-based bulk metallic glasses (BMGs) possess excellent mechanical, physical, and chemical properties due to their amorphous structure without the crystal defects of dislocations and grain boundaries, giving rise to a new type of high-performance liner material [1-6]. It is well known that excellent liner materials have high density and good plasticity [7-9]. However, the brittleness of BMGs at room temperature and their reduced density limit their application as liner materials. Therefore, introducing high density and ductile elements to CuZr-based bulk metallic glass composites (BMGCs) is considered an effective method to improve the ductility and density of BMGs [10-12].

According to research [13, 14], Ta has a high density of up to 16.654 g·cm^{-3}. The melting point of Ta is over 3,000 K, which is significantly higher than the liquidus temperature of CuZr-based BMGs. When the liquid metal temperature falls below the melting point of Ta during the nonequilibrium solidification process, the ductile Ta solid solution precipitates. As the temperature decreases, the rest of the melt will solidify into an amorphous phase, and finally, BMGCs will be obtained. Therefore, Ta element with good plasticity and a high melting point is selected as the additional element, improving the density of CuZr-based BMGCs and enhancing the ductility of CuZr-based BMGCs. For example, when 6vol.% Ta particles were added to Cu-based alloys, the compressive fracture strength of the alloy was 1,800 MPa, and the plastic shrinkage deformation reached 25% [15]. Moreover, Li et al. [14] showed that when 10vol.% of Ta particles were added to CuZr-based BMGCs, the compressive fracture strength of composites was 1,850 MPa, and plastic deformation reached 22%. However, the effect of Ta-rich particles, including the volume fraction of Ta particles and the interface between Ta particles and the amorphous matrix, on the mechanical properties of CuZr-based BMGCs is still far from being understood.

In this study, based on previous results [16, 17], $(Cu_{43}Zr_{48}Al_9)_{98}Y_2$ BMG was chosen as the matrix BMG because of its high glass forming ability. The different volume fractions of Ta particles were added to the $(Cu_{43}Zr_{48}Al_9)_{98}Y_2$-based BMG to form the BMGCs, and their microstructure, thermal properties, and mechanical behavior were systematically investigated.

***Ke Yang**
Male, Ph.D., Research interest: amorphous alloys. He has participated in one project supported by the National Natural Science Foundation and three projects with the General Armament Department. To date, he has held two invention patents and has published more than ten academic papers.
E-mail: yangke311228@foxmail.com
Received: 2021-01-22; Accepted: 2021-11-05

2 Experiment

A two-step melting process was conducted. In a Ti-gettered Ar atmosphere, high purity Cu, Zr, Al, and Y raw metals were first arc-melted together to form a homogeneous alloy ingot. Then, the alloy ingots were re-melted with 3vol.%, 6vol.%, and 9vol.% Ta particles (with an average particle size of 25±5 μm) to obtain the target composite composition by arc-melting under a Ti-gettered Ar atmosphere. The liquid alloy was suction cast into the water-cooled Cu mold after complete melting to form alloy rods with a diameter of 3 mm.

The thermal parameters of the specimens were determined by a differential scanning calorimeter (DSC, METTLER-TOLEDO TGA/DSC1) under a high-purity argon atmosphere at a heating rate of 20 $K\cdot min^{-1}$. Energy-dispersive X-ray spectroscopy was used to determine the composition of Ta-rich particles in BMGCs. The phase constitution and microstructures of the specimens were analyzed using X-ray diffraction (XRD, SHIMADU XRD-6000, Cu Kα) and scanning electron microscopy (SEM, FEI Quanta 400 FEG), respectively. The hardness of the specimens was tested by a 402MVD hardness tester. The compression performance of the specimens with size of Φ3 mm×6 mm cut from the cylindrical rods using a diamond slicing instrument was tested on a CMT5305 testing machine with a strain rate of 1×10^{-4} s^{-1}. The fracture surface of the compression specimens was also examined by SEM. The estimated mean interparticle free spacing of Ta particles in the composites was a statistical average of SEM images by Image-Pro Plus image analysis software.

3 Results and discussion

3.1 Thermal properties of Ta/$(Cu_{43}Zr_{48}Al_9)_{98}Y_2$

The DSC curves of the $(Cu_{43}Zr_{48}Al_9)_{98}Y_2$ base BMG and the Ta/$(Cu_{43}Zr_{48}Al_9)_{98}Y_2$ BMGCs with 3vol.%, 6vol.%, and 9vol.% Ta particles are shown in Fig. 1. All DSC curves exhibit an endothermic glass transition and one exothermic peak corresponding to the successive transformation from a metastable supercooled liquid state to equilibrium crystalline intermetallic phases during the continuous heating process. The glass transition temperature, T_g, and crystallization temperature, T_x, of BMGCs are indicated by arrows in their respective DSC curves. The values of T_g, T_x, and supercooled liquid range ΔT_x ($\Delta T_x = T_x - T_g$), are shown in Table 1. Figure 1 and Table 1 show that T_g and T_x of the BMGCs with Ta particles are higher than those of the base $(Cu_{43}Zr_{48}Al_9)_{98}Y_2$ alloy and the ΔT_x of the BMGCs with Ta particles is lower than that of the base BMG. It is found that T_g, T_x, and ΔT_x of the composites with Ta particles do not significantly change with an increase in the Ta volume fraction. Thus, Ta/$(Cu_{43}Zr_{48}Al_9)_{98}Y_2$ BMGCs maintain similar thermal properties with $(Cu_{43}Zr_{48}Al_9)_{98}Y_2$ base BMG.

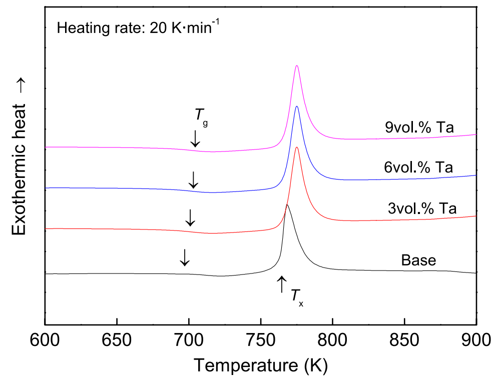

Fig. 1: DSC curves of base BMG and BMGCs with different volume fractions of Ta particles

Table 1: Thermal analysis data of base BMG and BMGCs with different volume fractions of Ta particles

Composition	T_g (K)	T_x (K)	ΔT_x (K)
Base	696	770	74
3vol.% Ta	704	772	68
6vol.% Ta	705	773	68
9vol.% Ta	707	774	67

3.2 Phase constitution and microstructure of Ta/$(Cu_{43}Zr_{48}Al_9)_{98}Y_2$

The XRD patterns of the $(Cu_{43}Zr_{48}Al_9)_{98}Y_2$ base BMG and the BMGCs with 3vol.%, 6vol.%, and 9vol.% Ta particles are shown in Fig. 2. The XRD pattern of the base BMG shows a broad, amorphous peak in the 2θ range of 35°–45°, which represents a completely amorphous structure. However, the aboard peak of the amorphous matrix superimposed with the crystalline peaks of Ta-rich particles can be seen for the BMGCs with Ta. The intensity of the crystalline peaks gradually increases with an increase in the Ta content. Energy-dispersive X-ray spectroscopy analysis determines the composition of Ta-rich particles in BMGCs, which is approximately $Ta_{90}Cu_3Zr_6Al_1$ (at.%). Cu and Ta are immiscible in Cu-Zr-Al-Y-Ta alloy, which promotes the aggregation and precipitation of Ta particles in the matrix. Furthermore, Ta will

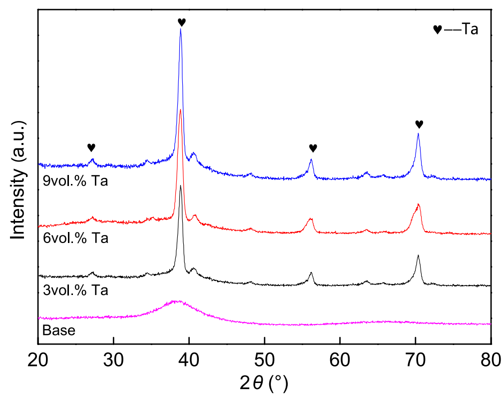

Fig. 2: XRD patterns of base BMG and BMGCs with different volume fractions of Ta particles

remain in the solid-state during the remelting process due to its high melting point (much higher than the liquidus temperature of CuZr-based BMGs). Therefore, these two factors lead to the precipitation of the Ta-rich phase. The SEM images of BMGCs with different volume fractions of Ta particles are shown in Fig. 3. It is observed from Fig. 3 that the white area is Ta-rich particles and the gray area is a glassy matrix. The estimated final volume fraction of the Ta particles in the composite using image analysis software is found to be close to the initial addition. The mean interparticle free spacing of Ta-rich particles is predicted to be 68±10 μm, 52±10 μm, and 33±8 μm for BMGCs with 3vol.%, 6vol.%, and 9vol.% Ta particles, respectively.

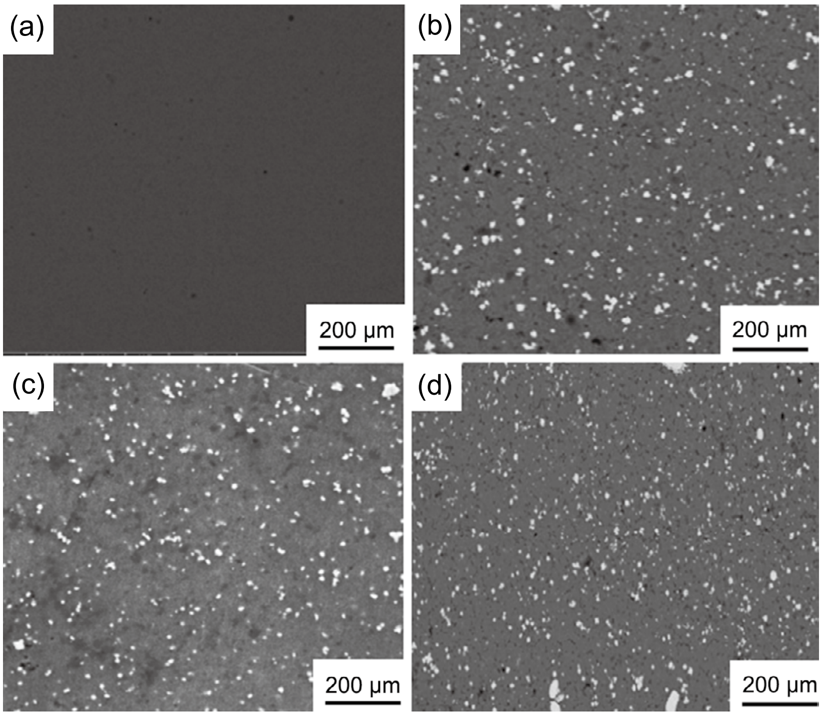

Fig. 3: SEM micrographs of base BMG and BMGCs with different volume fractions of Ta particles: (a) base; (b) 3vol.%; (c) 6vol.%; (d) 9vol.%

3.3 Mechanical properties of Ta/$(Cu_{43}Zr_{48}Al_9)_{98}Y_2$

The hardness values of the $(Cu_{43}Zr_{48}Al_9)_{98}Y_2$ base BMG and Ta/$(Cu_{43}Zr_{48}Al_9)_{98}Y_2$ BMGCs are shown in Table 2. The test results show that the hardness of the Ta/$(Cu_{43}Zr_{48}Al_9)_{98}Y_2$ BMGCs does not change much by the addition of Ta; these BMGCs all have hardness around 530–560 HV.

Additionally, the compressive stress-strain curves of the BMGCs with different volume fractions of Ta are shown in Fig. 4. The compressive properties for the BMGCs are listed in Table 3. The addition of Ta particles significantly improves the plastic deformation of the BMGCs. As shown in Fig. 4 and Table 3, the fracture strength, yield strength and plastic strain of the BMGCs increase with an increase in the volume fraction of Ta particles. The yield strength and fracture strength increase from 2,033 MPa and 2,134 MPa for the $(Cu_{43}Zr_{48}Al_9)_{98}Y_2$ base BMG up to 2,216 MPa and 2,260 MPa for the BMGCs with 9vol.% Ta, respectively. The plastic strain increases from 1.8% for the $(Cu_{43}Zr_{48}Al_9)_{98}Y_2$ base BMG up to 15.7% for the BMGCs with 9vol.% Ta because the closed zone between particles shrinks with an increase in Ta volume fraction, which may limit the expansion of the shear zone and hinder the brittle fracture of the BMGCs. Thus, Ta content greatly affects the strength and plasticity of Ta/$(Cu_{43}Zr_{48}Al_9)_{98}Y_2$ BMGCs, which is similar to the findings of Li et al [15].

Table 2: Hardness of base BMG and BMGCs with different volume fractions of Ta particles

Composition	HV
Base	554
3vol.% Ta	530
6vol.% Ta	560
9vol.% Ta	549

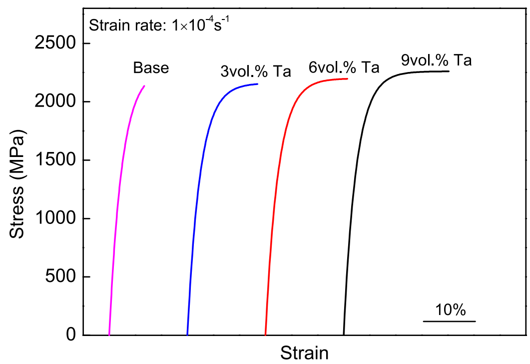

Fig. 4: Compressive stress-strain curves of Ta/$(Cu_{43}Zr_{48}Al_9)_{98}Y_2$ BMGCs

Table 3: Mechanical properties of BMG and BMGCs with different volume fractions of Ta particles

Composition	Yield strength (MPa)	Fracture strength (MPa)	Plastic strain (%)
Base	2,033	2,134	1.8
3vol.% Ta	2,096	2,152	6.4
6vol.% Ta	2,154	2,195	11.2
9vol.% Ta	2,216	2,260	15.7

Mechanical test results show that the addition of Ta leads to a remarkable improvement of both strength and plastic strain under uniaxial compression (shown in Fig. 4 and Table 3). It is well known that the introduction of the second ductile phase in the amorphous matrix is a universal approach to enhance the plasticity of a single phase of BMG [14, 18, 19]. Figure 5 shows SEM images of the specimen fracture surface for the BMGC with 6vol.% Ta. The BMGC breaks along the shear direction, with a shear fracture angle of 43°, as shown in Fig. 5(a). In theory, it is generated by the fault surface with the maximum shear stress, but in practice, there are multiple shear bands [18]. It is observed that multiple shear bands intersect with Ta particles near the fracture surface, as shown in Fig. 5(b). This result indicates a strong interaction between Ta particles and shear bands that is induced by the amorphous matrix. The deformation of ductile Ta particles releases a large amount of stress concentration and absorbs energy, hindering the expansion of shear bands in the amorphous matrix.

The compression fracture morphology of the $(Cu_{43}Zr_{48}Al_9)_{98}Y_2$ base BMG and Ta/$(Cu_{43}Zr_{48}Al_9)_{98}Y_2$ BMGCs with different volume fractions of Ta is shown in Fig. 6. The entire fracture surface of the $(Cu_{43}Zr_{48}Al_9)_{98}Y_2$ base BMG exhibits a uniform vein-like pattern which is the typical amorphous alloy fracture morphology, as shown in Fig. 6(a). However, the fracture surface of the BMGCs shows a mixed morphology, including a vein-like pattern and rough regions [Figs. 6(b)–(d)], which differs from the compressive fracture surface of the base BMG [16]. The locally melted region is observed on the fracture surface, implying that a large amount of strain along the shear band results in localized melting before fracture. Moreover, the rough region in the fracture surface of the BMGCs indicates that the shear bands are highly branched, and the movement of shear bands is rather rugged, which indicates a strong interaction between shear bands and Ta particles, this can improve the plasticity.

The plastic deformation of the $(Cu_{43}Zr_{48}Al_9)_{98}Y_2$-based BMG and Ta/$(Cu_{43}Zr_{48}Al_9)_{98}Y_2$ BMGCs is mainly caused by the shear band in the amorphous matrix. Especially in Ta/$(Cu_{43}Zr_{48}Al_9)_{98}Y_2$ BMGCs, the shear band is not free to expand or run away, but is often arrested at the amorphous matrix and Ta interface. The shear band's traveling distance (i.e., mean free path) is limited by the interparticle spacing between Ta particles. For a given Ta particle size, with an increase in the Ta particle volume fraction, the interfacial area increases, the interparticle spacing becomes smaller, and the mean free path also becomes smaller. The interparticle spacing is a valid parameter for analyzing the mean free path of the shear bands [20]. The smaller mean free path leads to higher plastic deformation. In Ta/$(Cu_{43}Zr_{48}Al_9)_{98}Y_2$ BMGCs, the BMGC with 9vol.% Ta particles has superior mechanical performance with up to 15.7% compressive plastic strain, 2,216 MPa yield strength, and 2,260 MPa fracture strength.

The correlation between the yield stress σ_y and the scale of plastic process zone R_P can be given as follows [21]:

$$R_P = \left(\frac{1}{6\pi}\right)\left(\frac{K_C}{\sigma_y}\right)^2 \tag{1}$$

where K_C is the fracture toughness. For a tougher $Zr_{41}Ti_{14}Cu_{12.5}Ni_{10}Be_{22.5}$

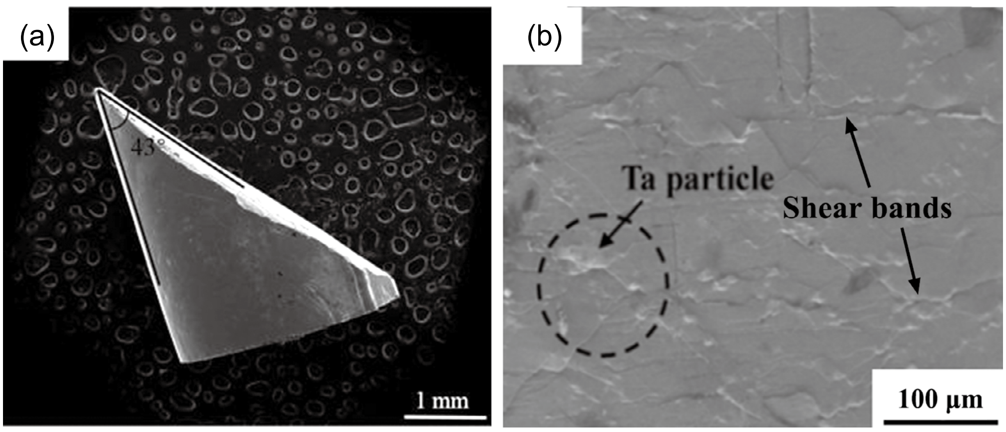

Fig. 5: SEM images of the surface (a) and near the fracture area (b) of BMGCs with 6vol.% Ta particles

amorphous alloy [21], the K_C is 86 MPa $\sqrt{m}$ and the yield strength is 1,800 MPa, which shows the large plastic zone size (approximately 60 μm), and significant crack bifurcation and branching, leading to high plasticity. In contrast, brittle $Mg_{65}Cu_{25}Tb_{10}$ amorphous alloy with K_C=2 MPa $\sqrt{m}$ and yield strength of 660 MPa, only shows a very small plastic zone size, approximately 0.1 μm [21]. For the $(Cu_{43}Zr_{48}Al_9)_{98}Y_2$ base BMG, the yield strength is approximately 2,000 MPa, and the assumed fracture toughness is 70 MPa $\sqrt{m}$ [22]. According to Eq. (1), its plastic zone size is approximately 75 μm, which is clearly larger than the mean interparticle free spacing of Ta particles (confinement zone sizes of 68±10, 52±10, and 33±8 μm for the Ta/$(Cu_{43}Zr_{48}Al_9)_{98}Y_2$ BMGCs with 3vol.%, 6vol.%, and 9vol.% Ta particles, respectively). Therefore, the confinement region of Ta particles will provide plastic shielding of an opening crack tip to limit the expansion of the shear zone, which allows one to avoid catastrophic crack propagation [23]. The presence of Ta particles will cause shear zone branching, devouring, and even termination [Fig. 5(b)], all of which result in increased plasticity.

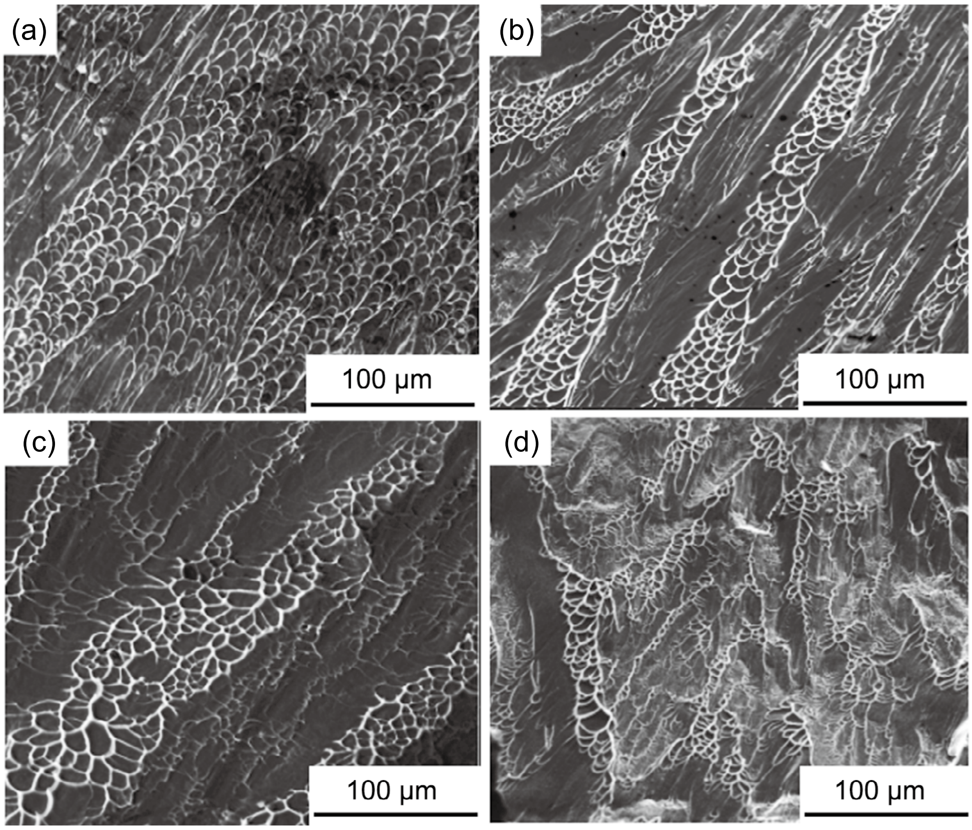

Fig. 6: SEM images of fracture feature for base BMG and BMGCs with different volume fractions of Ta particles: (a) base; (b) 3vol.%; (c) 6vol.%; (d) 9vol.%

4 Conclusions

(1) T_g, T_x, and ΔT_x of the $(Cu_{43}Zr_{48}Al_9)_{98}Y_2$ BMGCs with Ta particles do not significantly change with an increase in the Ta particles volume fraction. Thus, these Ta particles reinforced BMGCs exhibit similar thermal properties as that of the $(Cu_{43}Zr_{48}Al_9)_{98}Y_2$ base BMG.

(2) The hardness of the Ta/$(Cu_{43}Zr_{48}Al_9)_{98}Y_2$ BMGCs does not change much by the addition of Ta, these BMGCs all have hardness around 530–560 HV. The fracture strength, yield strength and plastic deformation of the BMGCs increase with an increase in the Ta particles. The superior mechanical performance with up to 15.7% compressive plastic strain, 2,216 MPa yield strength, and 2,260 MPa fracture strength at room temperature can be obtained for the BMGC with 9vol.% Ta particles.

(3) The deformation mechanism of the Ta/$(Cu_{43}Zr_{48}Al_9)_{98}Y_2$ BMGCs changes from single shear band without Ta particles to multiple shear bands with Ta particles. The plastic zone size of the BMGCs is apparently larger than the mean inter-particle free spacing of Ta particles. Therefore, the confinement region of Ta particles will provide plastic shielding of an opening crack tip to limit the expansion of the shear zone. This results in the formation of multiple shear bands around the Ta-rich particles and decreases the stress concentration for further propagation of the shear band, improving the BMGCs' plasticity dramatically.

Acknowledgement

This work was financially supported by the President Fund of Xi'an Technological University (Grant No. 0852-302021407).

References

[1] Li P Y, Meng F Y, Wang Y S, et al. Glass forming ability and thermodynamic properties in novel La-Al-Cu-Co bulk metallic glasses. Journal of Rare Earths, 2015, 33(9): 972–976.

[2] Francisco G C, Luis R A, Conrado R M A, et al. Comparative study between two die cast methods for processing Cu-Zr-Al bulk metallic glasses. Journal of Materials Research and Technology, 2013, 2(2): 125–129.

[3] Mandal S, Kailath A J. Enhanced plasticity of Cu-Zr-Ti bulk metallic glass and its correlation with fragility. Metallurgical and Materials Transactions A, 2019, 50(1): 199–208.

[4] Wu J L, Peng Z. Effects of microadditions on glass transition and hardness of Cu-based bulk metallic glasses. Applied Physics A, 2018, 124(9): 632.

[5] Deng L, Zhou B W, Yang H S, et al. Roles of minor rare-earth elements addition in formation and properties of Cu-Zr-Al bulk metallic glasses. Journal of Alloys and Compounds, 2015, 632: 429–434.

[6] Wu Y, Wang H, Wu H H, et al. Formation of Cu-Zr-Al bulk metallic glass composites with improved tensile properties. Acta Materialia, 2011, 59(8): 2928–2936.

[7] Manfred H. Liners for shaped charges. Journal of Battlefield Technology, 2001, 4(3): 1–11.

[8] Lane M W, Murray C E, McFeely F R, et al. Liner materials for direct electrodeposition of Cu. Applied Physics Letters, 2003, 83(12): 2330–02332.

[9] Yin J P, Shi Z X, Chen J, et al. Smooth particle hydrodynamics-based characteristics of a shaped jet from different materials. Strength of Materials, 2019, 51(1): 85–94.

[10] Wei G, Hidemi K. Development and microstructure optimization of Mg-based metallic glass matrix composites with in situ B_2-NiTi dispersoids. Materials and Design, 2015, 83: 238–248.

[11] Qin C L, Zhang W, Asami K, et al. A novel Cu-based BMG composite with high corrosion resistance and excellent mechanical properties. Acta Materialia, 2006, 54(14): 3713–3719.

[12] Qin C L, Kimura H, Zhang W, et al. Excellent mechanical properties of Cu-Hf-Ti-Ta bulk glassy alloys containing in-situ dendrite Ta-based BCC phase. Materials Transactions, 2004, 45(9): 2936–2940.

[13] Liu Z Q, Lia R, Liu G, et al. Microstructural tailoring and improvement of mechanical properties in CuZr-based bulk metallic glass composites. Acta Materialia, 2012, 60: 3128–3139.

[14] Liu L, Chan K C, Sun M, et al. The effect of the addition of Ta on the structure, crystallization and mechanical properties of Zr-Cu-Ni-Al-Ta bulk metallic glasses. Materials Science and Engineering A, 2007, 445–446: 697–706.

[15] Li J B, Jang J S C, Li C, et al. Significant plasticity enhancement of ZrCu-based bulk metallic glass composite dispersed by in situ and ex situ Ta particles. Materials Science and Engineering A, 2012, 551: 249–254.

[16] Yang K, Fan X H, Li B, et al. Solidification microstructures of Cu-Zr-Al-Y BMG produced by casting in a wedge-shaped copper mold. International Journal of Materials Research, 2017, 108(3): 202–207.

[17] Li B, Li Y H, Yang K, et al. Effect of yttrium addition on the non-isothermal crystallization kinetics and fragility of Cu-Zr-Al bulk metallic glass. Thermochimica Acta, 2016, 642: 105–110.

[18] Choi-Yim H, Johnson W L. Bulk metallic glass matrix composites. Applied Physics Letters, 1997, 71: 3808–3810.

[19] Hays C C, Kim C P, Johnson W. Microstructure controlled shear band pattern formation and enhanced plasticity of bulk metallic glasses containing in situ formed ductile phase dendrite dispersions. Physical Review Letters, 2000, 84(13): 2901–2904.

[20] He G, Zhang Z F, Loser W, et al. Effect of Ta on glass formation, thermal stability and mechanical properties of a $Zr_{52.25}Cu_{28.5}Ni_{4.75}Al_{9.5}Ta_5$ bulk metallic glass. Acta Materialia, 2003, 51: 2383–2395.

[21] Xi X K, Zhao D Q, Pan M X, et al. Fracture of brittle metallic glasses: Brittleness or plasticity. Physical Review Letters, 2005, 94(12): 125510.

[22] Kawashima A, Kurishita H, Kimura H, et al. Fracture toughness of $Zr_{55}Al_{10}Ni_5Cu_{30}$ bulk metallic glass by 3-point bend testing. Materials Transactions, 2005, 46(7): 1725–1732.

[23] Hofmann D C, Suh J Y, Wiest A, et al. Designing metallic glass matrix composites with high toughness and tensile ductility. Nature, 2008, 451(28): 1085–1089.